Inorg. Chem. **2008**, *47*, 645–655

Synthesis, Characterization, and Study of Octanuclear Iron-Oxo Clusters Containing a Redox-Active Fe_4O_4-Cubane Core

Peter Baran,[†,‡] Roman Boča,[§] Indranil Chakraborty,[†] John Giapintzakis,[∥] Radovan Herchel,[⊥,#] Qing Huang,[†] John E. McGrady,[▽] Raphael G. Raptis,*[,†] Yiannis Sanakis,[○] and Athanasios Simopoulos[○]

Department of Chemistry and the Institute of Functional Nanomaterials, University of Puerto Rico, San Juan, Puerto Rico 00931-3346, Department of Inorganic Chemistry, Slovak University of Technology, SK-812 37 Bratislava, Slovakia, Department of Mechanical and Manufacturing Engineering, University of Cyprus, 75 Kallipoleos Avenue, P.O. Box 20537, 1678 Nicosia, Cyprus, Department of Chemistry, University of SS. Cyril and Methodius, Trnava, SK-91701, Slovakia, Department of Inorganic Chemistry, Palacký University, Křížkovského 10, CZ-77147 Olomouc, Czech Republic, WestCHEM, Department of Chemistry, University of Glasgow, Glasgow G12 8QQ, U.K., and Institute of Materials Science, NCSR "Demokritos", 15310 Aghia Paraskevi, Athens, Greece

Received October 13, 2007

A one-pot synthetic procedure yields the octanuclear Fe^{III} complexes $Fe_8(\mu_4\text{-}O)_4(\mu\text{-}pz^*)_{12}X_4$, where X = Cl and pz* = pyrazolate anion (pz = $C_3H_3N_2^-$) (**1**), 4-Cl-pz (**2**), and 4-Me-pz (**3**) or X = Br and pz* = pz (**4**). The crystal structures of complexes **1**–**4**, determined by X-ray diffraction, show an Fe_4O_4-cubane core encapsulated in a shell composed of four interwoven $Fe(\mu\text{-}pz^*)_3X$ units. Complexes **1**–**4** have been characterized by ^1H NMR, infrared, and Raman spectroscopies. Mössbauer spectroscopic analysis distinguishes the cubane and outer Fe^{III} centers by their different isomer shift and quadrupole splitting values. Electrochemical analyses by cyclic voltammetry show four consecutive, closely spaced, reversible reduction processes for each of the four complexes. Magnetic susceptibility studies, corroborated by density functional theory calculations, reveal weak antiferromagnetic coupling among the four cubane Fe centers and strong antiferromagnetic coupling between cubane and outer Fe atoms of **1**. The structural similarity between the antiferromagnetic $Fe_8(\mu_4\text{-}O)_4$ core of **1**–**4** and the antiferromagnetic units contained in the minerals ferrihydrite and maghemite is demonstrated by X-ray and Mössbauer data.

Introduction

We describe here the syntheses, structural characterization, and physical properties of four octanuclear Fe^{III} complexes containing a common redox-active Fe_4O_4-cubane core, along with arguments supporting the suggestion that a future discovery of an electron-transfer protein with a Fe_4O_4 active center is not an unreasonable expectation. Iron−sulfur cubanes able to cycle between two (or more) oxidation states constitute the electron-transfer components of several ferredoxins involved in biological redox processes.[1] Consequently, the study of model complexes containing Fe_4S_4-cubane cores

* To whom correspondence should be addressed. E-mail: raphael@adam.uprr.pr.
[†] University of Puerto Rico.
[‡] Present address: Department of Chemistry, Juniata College, Huntingdon, PA 16652.
[§] Slovak University of Technology.
[∥] University of Cyprus.
[⊥] University of SS. Cyril and Methodius.
[#] Palacký University.
[▽] University of Glasgow.
[○] NCSR "Demokritos".

(1) (a) Beinert, H.; Holm, R. H.; Münck, E. *Science*, **1997**, *277*, 653. (b) George, D. G.; Hunt, L. T.; Yeh, L. S.; Baker, W. C. *J. Mol. Evol.* **1985**, 22, 20. (c) Zhou, Z. H.; Adams, M. W. W. *Biochemistry* **1997**, *36*, 10892. (d) Ma, K.; Hutchins, A.; Sung, S. J. S.; Adams, M. W. W. *Proc. Natl. Acad. Sci. U.S.A.* **1997**, *94*, 9608. (e) Kisker, C.; Schindelin, H.; Rees, D. C. *Annu. Rev. Biochem.* **1997**, *66*, 233. (f) Tainer, J. A.; Thayer, M. M.; Cunningham, R. P.; *Curr. Opin. Struct. Biol.* **1995**, *5*, *20*. (g) Pereira, I. A. C.; Romao, C. V.; Xavier, A. V.; LeGall, J.; Teixeira, M. J. *J. Biol. Inorg. Chem.* **1998**, *3*, 494. (h) Peters, J. W.; Lanzilotta, W. N.; Lemon, B. J.; Seefeldt, L. C. *Science* **1998**, *282*, 1853. (i) Nicolet, Y.; Piras, C.; Legrand, P.; Hatchikian, E. C.; Fontecilla, Camps, J. C. *Structure* **1999**, *7*, 13. (j) Breiter, D. R.; Meyer, T. E.; Rayment, I.; Holden, H. M. *J. Biol. Chem.* **1991**, *266*, 18660. (k) Kim, J.; Rees, D. C. *Biochemistry* **1994**, *33*, 389. (l) Cammack, R.; Fernandez, V. M.; Hatchikia, E. C. *Methods. Enzymol.* **1994**, *243*, 43. (m) Crane, B. R.; Getzoff, E. D. *Curr. Opin. Struct. Biol.* **1996**, *6*, 744.

10.1021/ic7020337 CCC: $40.75
Published on Web 12/14/2007

has been a central theme of bioinorganic chemistry over the last 30 years.[2] While no redox-active Fe_4O_4-cubane core has been unequivocally characterized in a metalloprotein, examples of protein active centers consisting of Fe/O-containing cubanes are known: A unique redox-active $Fe_4O_2S_2$ cluster has been recognized in the active core of hybrid cluster protein (HCP, formerly termed prismane protein).[3] The HCP of *E. coli* catalyzes the two-electron reduction of hydroxylamine to ammonia.[4] Similar hydroxylamine reductase activity results from the insertion of Fe into the vacant site of Ni-deficient carbon monoxide dehydrogenase (Ni−CODH, with an Fe_3NiO_4-cubane core),[5] creating in a sense Fe−CODH.[4] In a recent Fe K-edge X-ray absorption spectroscopic study, Hogdson et al. have shown that a protein isolated from the blood of *Perophora annectens* contains a Fe_4O_4 core in either a cubane or a ladder arrangement, with the authors leaning toward the cubane assignment.[6] The absence of a well characterized Fe_4O_4 electron-transfer protein cannot simply be due to a scarcity of components—oxo and hydroxo ligands are readily available in Nature and metal-oxo active cores are present in numerous metalloproteins, including the Fe_2O_2 cores of ribonucleotide reductase, purple acid phosphatase, and soluble methane monooxygenase.[7] A structure containing fused cubanes with six-coordinate Fe centers is also one of the possible models consistent with the extended X-ray absorption fine structure studies of ferritin, the mammalian iron-storage protein, containing a few thousand Fe^{III} centers.[8]

Several synthetic iron complexes containing the Fe_4O_4 motif with Fe^{II} or mixed-valent $Fe^{II/III}$ centers have been reported to date.[9−19] These are either Fe_4O_4-carboxylate complexes or larger polynuclear carboxylates containing Fe_4O_4 units. Our contribution to this field consists of a preliminary account of the simple, one-pot synthesis and structural characterization of an octanuclear Fe^{III} cluster, $Fe_8(\mu_4\text{-}O)_4(\mu\text{-}pz)_{12}Cl_4$ (pz = pyrazolato anion, $C_3H_3N_2^-$), **1**, containing an $Fe^{III}_4O_4$-cubane core.[20] The latter, along with the recently characterized $[Fe_8^{III}O_4(sao)_8(py)_4]\cdot 4py$,[19] (sao = salicylaldoximato; py = pyridine) constitute the only examples of all-ferric oxo cubanes. Furthermore, we have shown that **1** can reversibly accept up to four electrons in four consecutive electrochemical steps, spaced approximately 0.35 V from each other.[20] The first reduction occurs at the modest potential of −0.43 V, while the fourth one lies at −1.38 V (versus Fc^+/Fc); compound **1** can shuttle four electrons across a redox potential window of ∼1.1 V. Consequently, the redox properties of **1** show it to be a more efficient electron-transfer agent than any of the naturally occurring or synthetic Fe_4S_4 clusters.[21] The question that arises, then, is the following: Why has Nature apparently ignored such a simple and efficient redox catalyst in favor of its sulfur analogues? It can be argued that Nature's preference for sulfur-based cubanes arises simply because ferredoxins are believed to have evolved during a prephotosynthetic geological period in an anoxic, sulfur-rich environment.[22] However, proteins are able to mutate to adapt to their changing environment by switching from depleted to readily available elements. For example, oxygen-for-sulfur substitution is known in the case of rubredoxin from *C. pasteurianum*, which switches from an $Fe(S\text{-}cyst)_4$ core to a $Fe(S\text{-}cyst)_3(OH)$ one, while the $Fe_4(S\text{-}cys)_4$ active center of *C. vinosum* switches to $Fe_4(S\text{-}cys)_3(O\text{-}ser)$.[23] Consequently, it is quite possible that an initially sulfur-based multi-iron protein may later have evolved into an oxygen-based one. Noting also that many metalloproteins remain to be discovered, Lippard et al. and we have suggested that an electron-transfer protein with a Fe_4O_4 active center may be recognized in the future.[15,20]

Continuing our studies of the octanuclear cluster **1**, we report here the magnetic susceptibility, density functional theory (DFT), and infrared, Raman, ^{1}H NMR, and Mössbauer

(2) Rao, P. V.; Holm, R. H. *Chem. Rev.* **2004**, *104*, 527.
(3) (a) Arendsen, A. F.; Hadden, J.; Card, G.; McAlpine, A. S.; Bailey, S.; Zaitsev, V.; Duke, E. H. M.; Lindley, P. F.; Kröckel, M.; Trautwein, A. X.; Feiters, M. C.; Charnock, J. M.; Garner, C. D.; Marritt, S. J.; Thompson, M. K.; Kooter, I. M.; Johnson, M. K.; van den Berg, W. A. M.; van Dongen, W. M. A. M.; Hagen, W. R. *J. Biol. Inorg. Chem.* **1998**, *3*, 81. (b) van den Berg, W. A. M.; Hagen, W. R.; van Dongen, W. M. A. M. *Eur. J. Biochem.* **2000**, *267*, 666.
(4) (a) Wolfe, M. T.; Heo, J.; Gararelli, J. S.; Ludden, P. W. *J. Bacteriol.* **2002**, 5898. (b) Cabello, P.; Pino, C.; Olmos-Mira, M. F.; Castillo, F.; Roldan, M. D.; Moreno-Vivian, C. *J. Biol. Chem.* **2004**, *279*, 45485.
(5) Dobbek, H.; Svetlitchnyi, V.; Gremer, L.; Huber, R.; Meyer, O. *Science* **2001**, *293*, 1281.
(6) Fank, P.; De Tomaso, A.; Hedman, B.; Hodgson, K. O. *Inorg. Chem.* **2006**, *45*, 3920.
(7) (a) Wallar, B. J.; Lipscomb, J. D. *Chem. Rev.* **1996**, *96*, 2625. (b) Klabunde, T.; Krebs, B. *Struct. Bond.* **1997**, *89*, 177. (c) Lange, S. J.; Que, L., Jr. *Curr. Opin. Chem. Biol.* **1998**, *2*, 159. (d) Westerheide, L.; Pascaly, M.; Krebs, B. *Curr. Opin. Chem. Biol.* **2000**, *4*, 235 and references therein.
(8) Ford, G. C.; Harrison, P. M.; Rice, D. W.; Smith, J. M. A.; Treffry, A.; White, J. L.; Yariv, J. *Philos. Trans. R. Soc. London, Ser. B* **1984**, *304*, 551.
(9) Shoner, S. C.; Power, P. P. *Inorg. Chem.* **1992**, *31*, 1001.
(10) Taft, K. L.; Caneschi, A.; Pence, L. E.; Delfs, C. D.; Papaefthymiou, G. C.; Lippard, S. J. *J. Am. Chem. Soc.* **1993**, *115*, 11753.
(11) Taft, L.; Papaefthymiou, G. C.; Lippard, S. J. *Science* **1993**, *259*, 1302.
(12) Taft, K. L.; Papaefthymiou, G. C.; Lippard, S. J. *Inorg. Chem.* **1994**, *33*, 1510.
(13) Dell'Amico, D. B.; Boschi, D.; Calderazo, F.; Ianelli, S.; Labella, L.; Marchetti.; Pelizzi, G.; Quadrelli, E. G. F. *Inorg. Chim. Acta* **2000**, *300−302*, 882.
(14) (a) Oshio, H.; Hoshino, N.; Ito, T. *J. Am. Chem. Soc.* **2000**, *122*, 12602. (b) Oshio, H.; Hoshino, N.; Ito, T.; Nakano, M. *J. Am. Chem. Soc.* **2004**, *126*, 8805.
(15) Lee, D.; Sorace, L.; Caneschi, A.; Lippard, S. J. *Inorg. Chem.* **2001**, *40*, 6774.
(16) Clemente-Juan, J. M.; Mackiewicz, C.; Verelst, M.; Dahan, F.; Bousseksou, A.; Sanakis, Y.; Tuchagues, J.-P. *Inorg. Chem.* **2002**, *41*, 1478.
(17) Abrahams, B. F.; Hudson, T. A.; Robson, R. *J. Am. Chem. Soc.* **2004**, *126*, 8624.
(18) Hudson, T. A.; Berry, K. J.; Moubaraki, B.; Murray, K.; Robson, R. *Inorg. Chem.* **2006**, *45*, 3549.
(19) Gass, I. A.; Milios, C. J.; Whittaker, A. G.; Fabiani, F. P. A.; Parsons, S.; Murrie, M.; Perlepes, S. P.; Brechin, E. K. *Inorg. Chem.* **2006**, *45*, 5281.
(20) Raptis, R. G.; Georgakaki, I. P.; Hockless, D. C. R. *Angew. Chem., Int. Ed.* **1999**, *38*, 1632.
(21) (a) Stephens, P. J.; Jollie, D. R.; Warshel, A. *Chem. Rev.* **1996**, *96*, 2491. (b) Zanello, P. A. *Coord. Chem. Rev.* **1988**, *87*, 1. (c) Zanello, P. *Coord. Chem. Rev.* **1988**, *83*, 199.
(22) Martin, W.; Russell, M. J. *Philos. Trans. R. Soc. London, Ser. B.* **2003**, *358*, 59.
(23) (a) Xiao, Z. G.; Gardner, A. R.; Cross, M.; Maes, E. M.; Czernuszewicz, R. S.; Sola, M.; Wedd, A. G. *J. Biol. Inorg. Chem.* **2001**, *6*, 638. (b) Dilg, A. W. E.; Capozzi, F.; Mentler, M.; Iakovleva, O.; Luchinat, C.; Bertini, I.; Parak, F. G. *J. Biol. Inorg. Chem.* **2001**, *6*, 232. (c) Xiao, Z.; Lavery, M. J.; Ayhan, M.; Scrofani, S. D. B.; Wilce, M. C. J.; Guss, J. M.; Tregloan, P. A.; Goerge, G. N.; Wedd, A. G. *J. Am. Chem. Soc.* **1998**, *120*, 4135.

spectroscopic characterization of **1**, along with the syntheses, structural characterization, and electrochemical studies of its substituted-pyrazole derivatives $Fe_8(\mu_4\text{-}O)_4(\mu\text{-}pz^*)_{12}Cl_4$, where pz* = 4-Cl-pz (**2**) and 4-Me-pz (**3**), along with the bromo analogue $Fe_8(\mu_4\text{-}O)_4(\mu\text{-}pz)_{12}Br_4$, (**4**). These studies probe the electronic structure of the Fe_4O_4 motif and define its spectroscopic and magnetic "fingerprint", facilitating its possible future recognition in Nature.

Experimental Section

$FeCl_3$, $FeBr_3$, pyrazole (pzH), 4-Me-pyrazole (4-Me-pzH), NaH, and Et_3N were obtained from commercial sources and used as received. Napz was prepared from pzH and NaH. 4-Cl-pyrazole (4-Cl-pzH) was prepared by a literature method.[24] Solvents (CH_2Cl_2, methanol, acetone, diethyl ether, tetrahydrofuran, hexane) were purified by standard methods.[25]

$[Fe_8(\mu_4\text{-}O)_4(\mu\text{-}pz)_{12}Cl_4]$ (1). To a suspension of $FeCl_3$ (3.120 g, 19.23 mmol) in CH_2Cl_2 (200 mL) was added Napz (2.598 g, 28.85 mmol) under an Ar atmosphere with stirring. The reaction mixture was exposed to air, sealed, and kept under stirring at ambient temperature for 20 h. The resulting dark brown solution was then filtered, the filtrate was collected in a round-bottomed flask, and the solvent was evaporated under reduced pressure. The resulting solid was dissolved in the minimum amount of CH_2Cl_2 with which was charged a silica gel chromatographic column (60−120 mesh, Aldrich) prepared with toluene. The dark orange portion eluted with CH_2Cl_2 was collected in a round-bottomed flask, the solvent was removed in a rotary evaporator, and the product was air-dried, washed with dry MeOH, and then dried in a vacuum desiccator over $CaCl_2$. X-ray-quality dark red crystals were obtained upon recrystallization by slow Et_2O-vapor diffusion into a CH_2Cl_2 solution of **1**. Yield: 1.07 g (30%). UV−vis−NIR (CH_2Cl_2): λ_{max} = 360 nm (27 788 cm^{-1}), ϵ = 37 000 cm^{-1} mol^{-1} dm^3. IR (KBr disk): 1490(m), 1417(m), 1362(vs), 1268(vs), 1170(m), 1145(w), 1045(vs), 963(w), 915(w), 895(w), 871(w), 764(s), 615(m), 556(w), 478 (vs, br Fe−O). ^{1}H NMR (δ, ppm, $CDCl_3$): 42.2 (s, 1 H, ^{4}H), 10.5 (s, 1 H, ^{3}H), 3.5 (s, 1 H, ^{5}H).

$[Fe_8(\mu_4\text{-}O)_4(\mu\text{-}4\text{-}Cl\text{-}pz)_{12}Cl_4]$ (2). To a suspension of $FeCl_3$ (0.586 g, 3.61 mmol) in CH_2Cl_2 (200 mL) was added 4-Cl-pzH (0.556 g, 5.42 mmol) under an Ar atmosphere with stirring. To the resulting solution, Et_3N (0.629 mL, 4.52 mmol) was added dropwise with stirring under Ar. Then the reaction mixture was exposed to air, sealed, and kept under stirring at room temperature for 20 h. Then the resulting dark brown solution was filtered and worked up in a fashion similar to that described for **1**. X-ray-quality single crystals were grown by the slow evaporation of a CH_2Cl_2 solution of **2**. Yield: 0.338 g (40%). Anal. Calcd for $C_{40}H_{40}Cl_{18}Fe_8N_{24}O_4$: C, 22.36; H, 1.88; N, 15.64. Found: C, 22.61; H, 1.93; N, 15.36. UV−vis−NIR (CH_2Cl_2): λ_{max} = 363 nm (27 639 cm^{-1}). The ^{18}O isotopically labeled complex **2** was prepared as above, except that 0.05 mL of $H_2{}^{18}O$ was added to the reaction mixture under an Ar atmosphere instead of exposing it to the air. IR (KBr disk): 1384(m), 1354(m), 1315(w), 1297(vs), 1217(w), 1189(s), 1151(w), 1041(vs), 993(w), 967(m), 855(w), 608(s), 528(w), 475(vs, br Fe−O). ^{1}H NMR (δ, ppm, $CDCl_3$): 13.7 (s, 1 H, ^{3}H), 8.6 (s, 1 H, ^{5}H).

$[Fe_8(\mu_4\text{-}O)_4(\mu\text{-}4\text{-}Me\text{-}pz)_{12}Cl_4]$ (3). To a suspension of $FeCl_3$ (0. 967 g, 5.96 mmol) in CH_2Cl_2 (200 mL) was added 4-Me-pzH (1.48 mL, 17.9 mmol) under an Ar atmosphere with stirring. To the resulting solution, Et_3N (2.08 mL, 14.9 mmol) was added dropwise with stirring under Ar. Then the reaction mixture was exposed to air, sealed, and kept under stirring at room temperature for 20 h. Then the resulting dark brown solution was filtered and worked up in a fashion similar to that described for **1** and **2**. Yield: 0.698 g (57%). Anal. Calcd for $C_{48}H_{60}Cl_4Fe_8N_{24}O_4$: C, 35.46; H, 3.72; N, 20.68. Found: C, 36.14; H, 4.04; N, 20.53. UV−vis−NIR (CH_2Cl_2): λ_{max} = 376 nm (26 848 cm^{-1}). IR (KBr disk): 1389(w), 1355(s), 1311(s), 1216(w), 1165(m), 1054(vs), 1012(m), 846(m), 674(m), 617(s), 555(w), 478(vs, br Fe−O). ^{1}H NMR (δ, ppm, $CDCl_3$): 27.7 (s, 3 H, Me), 8.6 (s, 1 H, ^{3}H), 3.8 (s, 1 H, ^{5}H).

$[Fe_8(\mu_4\text{-}O)_4(\mu\text{-}pz)_{12}Br_4]$ (4). To a suspension of $FeBr_3$ (0.371 g, 1.26 mmol) in CH_2Cl_2 (15 mL) prepared under argon atmosphere was added solid pzH (0.256 g, 3.77 mmol) under air with stirring. To the red solution was added dropwise with stirring triethylamine (0.437 mL, 3.14 mmol). After stirring for 10 min, the mixture was filtered and the filtrate was placed into a Schlenk tube and stirred under nitrogen for 6 days. The volume of the reaction mixture was reduced to 5 mL under vacuum, and the mixture was stirred overnight and filtered under nitrogen. The filtrate was evaporated to dryness, washed with methanol (22 mL), and recrystallized from diethyl ether (40 mL) and subsequently from CH_2Cl_2 (6 mL). The product was collected by filtration, washed with methanol, and dried. Yield: 0.187 g (40%). Anal. Calcd for $C_{36}H_{36}Br_4Fe_8N_{24}O_4$: C, 26.44; H, 2.22; N, 20.56. Found: C, 26.24; H, 2.37; N, 20.38. UV−vis−NIR (CH_2Cl_2): λ_{max} = 399 nm (25 728 cm^{-1}). IR (KBr disk): 1491(m), 1417(m), 1362(s), 1266(s), 1230(w), 1168(s), 1076(w), 1044(vs), 764(s), 614(m), 552(w), 477(vs, br Fe−O). ^{1}H NMR (δ, ppm, $CDCl_3$): 42.9 (s, 1 H, ^{4}H), 10.7 (s, 1 H, ^{3}H), 1.0 (s, 1 H, ^{5}H).

Physical Measurements. The electronic spectra of the complexes in solution were recorded on a Varian CARY 500 scan instrument in the 200−2000 nm range. Infrared spectra (KBR and/or polyethylene pellets) were recorded on Nicolet 750 FTIR spectrophotometers. The Raman spectra of the solid samples in the form of powders were recorded at room temperature in backscattering geometry. Excitation at 488 nm was provided by a Lexel 95 Argon ion laser system, with applied laser power of 5−10 mW. The scattered light was dispersed by a triple-grating spectrometer (Jobin-Yvon, Edison, NJ), and the spectra were recorded by a liquid nitrogen cooled CCD camera (CCD3000 from Jobin-Yvon). ^{1}H NMR data were recorded on a Bruker AVANCE DRX-500 spectrometer. Electrochemical experiments were performed with a BAS CV 50 W voltammetric analyzer in 0.5 M Bu_4NPF_6/CH_2Cl_2 using a non-aqueous $Ag/AgNO_3$ reference electrode for which the ferrocene/ferricenium couple occurs at 2.00 V, Pt auxiliary electrode, and Pt working electrode. Mössbauer spectra were recorded with powdered samples of **1** with a constant-acceleration conventional spectrometer with a source of ^{57}Co (Rh matrix). Spectra in the 4.2−300 K range were obtained using Oxford cryostats. One cryostat was equipped with a superconducting magnet with the magnetic field perpendicular to the γ-rays. The spectra were analyzed by using the program *WMOSS* (Web Research, Edina, MN). Isomer shift values (δ) are reported relative to iron foil at 293 K. Temperature-dependent (2−298 K) magnetic susceptibility data were recorded on a SQUID magnetometer in an external magnetic field of 1 T. A correction to the underlying diamagnetism was estimated on the basis of Pascal constants as $\chi_{dia} = -7.45 \times 10^{-9}$ m^3 mol^{-1}.[26] The effective magnetic moment is calculated in SI units as $\mu_{eff}/\mu_B = 798[(\chi_{mol} - \chi_{dia})T]^{1/2}$.

Computational Methods. All calculations described in this paper were done using spin-unrestricted DFT as implemented in the

(24) Ehlert, M. K.; Rettig, S. J.; Storr, A.; Thompson, R. C.; Trotter, J. *Can. J. Chem.* **1991**, *69*, 432.
(25) Perrin, D. D.; Armarego, W. L. F.; Perrin, D. R. *Purification of Laboratory Chemicals*, 2nd ed.; Pergamon Press: New York, 1987.
(26) König, E. In *Landolt-Börstein*, Neue Serie; Springer: Berlin, 1966; Vol. 2, pp 1−16.

Table 1. Crystallographic Data for **1**−**4**

	1	**2**	**3**	**4**
formula	$C_{36}H_{36}Cl_4Fe_8N_{24}O_4$	$C_{36}H_{24}Cl_{16}Fe_8N_{24}O_4$	$C_{48}H_{62}Cl_4Fe_8N_{24}O_5$	$C_{36}H_{36}Br_4Fe_8N_{24}O_4$
cryst size, mm^3	0.22 × 0.20 × 0.08	0.29 × 0.29 × 0.15	0.12 × 0.08 × 0.02	0.34 × 0.05 × 0.04
fw	1457.49	1870.79	1643.82	1635.33
space group	$P2_1/n$ (No. 14)	$Fd\bar{3}$ (No. 203)	$P\bar{1}$ (No. 2)	$P2_1/n$ (No. 14)
a, Å	12.660(4)	25.934(2)	13.187(2)	12.847(2)
b, Å	21.519(6)	25.934(2)	13.601(2)	21.517(4)
c, Å	20.065(6)	25.934(2)	21.461(3)	20.030(4)
α, deg	90	90	87.545(3)	90
β, deg	92.976(5)	90	80.550(3)	93.492(3)
γ, deg	90	90	71.250(3)	90
V, $Å^3$	5459(3)	17442(2)	3595.2(10)	5526.5(17)
Z	4	8	2	4
T, K	298(2)	299(2)	302(2)	298(2)
ρ_{calcd}, g cm^{-3}	1.773	1.425	1.518	1.965
reflns collected/$2\theta_{max}$	23089/46.60	18404/55.96	16013/46.54	27721/50.50
unique reflns/$I > 2\sigma(I)$	7838/4631	1058/916	10301/4898	9938/4290
no. of params/restraints	685/0	67/0	833/0	685/0
μ(Mo Kα), mm^{-1}	2.321	1.825	1.772	4.991
F(000)	2912	7360	1668	3200
R1[a]/GOF[b]	0.0739/1.080	0.0431/1.292	0.0511/0.864	0.0589/0.933
wR2[c] ($I > 2\sigma(I)$)	0.1576	0.1552	0.1036	0.1058

[a] $I > 2\sigma(I)$. $R1 = \sum||F_o| - |F_c||/\sum|F_o|$. [b] $GOF = [\sum[w(F_o^2 - F_c^2)^2]/(n-p)]^{1/2}$. [c] $wR2 = [\sum[w(F_o^2 - F_c^2)^2]/\sum[w(F_o^2)^2]]^{1/2}$, where $w = 1/\sigma^2(F_o^2) + (aP)^2 + bP$, $P = (F_o^2 + 2F_c^2)/3$.

Gaussian 03 program, version D.02.[27] The B3LYP functional[28] was used throughout, in conjunction with the LANL2DZ basis set and associated effective core potential for Fe and Cl[29] and Dunning's D95 basis set for C, N, O, and H (856 basis functions in total).[30] The geometry of the Fe_8 cluster, $Fe_8(\mu_4\text{-}O)_4(\mu\text{-}pz)_{12}Cl_4$, was taken from our previously published paper[20], with no imposed symmetry constraints. Calculations on the broken-symmetry ($M_S = 0$) states were done using the converged high-spin ($M_S = 20$) density as an initial guess. Convergence to the required states with a local high-spin ($M_S = {}^5/_2$) configuration at each Fe center was then achieved in several steps using the guess=permute and guess=alter keywords.[31]

X-ray Crystallographic Data Collection and Refinement of the Structure. Suitable crystals for the X-ray measurement of **1** and **4** were obtained by the recrystallization of compounds from dichloromethane. For **2** and **3**, crystals of suitable quality were obtained directly from reactions similar to the ones described above. Crystals were selected from a mixture of cluster and side products, which crystallize as the first solid fraction directly after synthesis. That fraction typically contains well developed crystals of **2** or **3** together with colorless crystals of triethylammonium chloride.

X-ray diffraction data, collected from single crystals mounted atop glass fibers with a Siemens SMART 1K CCD diffractometer,[32a] were corrected for Lorentz and polarization effects.[32b] The structures were solved employing the *SHELX-90*[32c] program and refined by least-squares methods on F^2, via *SHELXTL-93*,[32d] incorporated in *SHELXTL*, version 5.1.[32e] Crystallographic details for **1**−**4** are summarized in Table 1.

Results and Discussion

The reactions of anhydrous FeX_3, X = Cl, Br, with pzH or 4-substituted pzH, in CH_2Cl_2 under an inert atmosphere give bright red products, which consist of mixtures of $FeX_3(pz^*H)_3$ and $[FeX_2(pz^*H)_4][FeX_4]$.[33] Further addition of NEt_3 to that mixture (to deprotonate the pzH ligands) and exposure to air results in the formation of dark red octanuclear clusters **1**−**4**, which have been characterized in solution as well as in the solid state. During the recrystallization of **2** and **3**, solvent molecules are trapped in interstitial cavities between the approximately spherical cluster molecules, resulting in the overall formula $[Fe_8(\mu_4\text{-}O)_4(\mu\text{-}4\text{-}Cl\text{-}pz)_{12}Cl_4]\cdot 2CH_2Cl_2\cdot {}^1/_2THF\cdot 4H_2O$ for **2** and $[Fe_8(\mu_4\text{-}O)_4(\mu\text{-}4\text{-}Me\text{-}pz)_{12}Cl_4]\cdot H_2O$ for **3**. The presence of solvent molecules in **2** was detected by ^1H NMR and IR spectroscopies and supported by elemental analysis results, while the water molecule of **3** was identified during the crystal structure study. Slow water loss causes crystal decomposition of **3** with time; its elemental analysis was calculated for a water-free sample.

X-ray Crystallography. The crystal structures of **1**−**4** (Figure 1) consist of a Fe_4O_4-cubane core encapsulated inside a shell of four $Fe(pz^*)_3Cl$ units (the crystal structure of the hexane solvate of **1** has been previously communicated).[20] Bond lengths and angles for **1**−**4** are summarized in Table 2. While the inorganic $Fe_8(\mu_4\text{-}O)_4$ cores of **1**−**4** are tetrahedral, the pzH ligands are tilted out of the mirror plane positions, thus reducing the point group symmetry from T_d to *T*; the four C_3 and three C_2-axes of the *T* point group are

(27) Frisch, M. J. et al. *Gaussian 03*, revision D.02; Gaussian, Inc.: Wallingford, CT, 2004. Full reference is given in the Supporting Information, Section S5.

(28) (a) Becke, A. D. *J. Chem. Phys.* **1993**, *98*, 5648. (b) Lee, C.; Yang, W.; Parr, R. G. *Phys. Rev. B: Condens. Matter Mater. Phys.* **1988**, *37*, 785. (c) Parr, R. G.; Yang, W. *Density Functional Theory of Atoms and Molecules*; Oxford University Press: New York, 1989.

(29) (a) Hay, P. J.; Wadt, W. R. *J. Chem. Phys.* **1985**, *82*, 270. (b) Wadt, W. R.; Hay, P. J. *J. Chem. Phys.* **1985**, *82*, 284.

(30) (a) Dunning, T. H., Jr. *J. Chem. Phys.* **1970**, *53*, 2823−2833. (b) Dunning, T. H., Jr.; Hay, P. J. In *Modern Theoretical Chemistry;* Schaefer, H. F., III, Ed.; Plenum: New York, 1976; Vol. 3, pp 1−28.

(31) http://www.gaussian.com.

(32) (a) *SMART-NT Software Reference Manual*, version 5.059; Bruker AXS, Inc.: Madison, WI, 1998. (b) *SAINT+ Software Reference Manual*, version 6.02; Bruker AXS, Inc.: Madison, WI, 1999. (c) Sheldrick, G. M. *SHELXS-90, Program for the Solution of Crystal Structure*; University of Göttingen: Göttingen, Germany, 1986. (d) Sheldrick, G. M. *SHELXL-97, Program for the Refinement of Crystal Structure*; University of Göttingen: Göttingen, Germany, 1997. (e) *SHELXTL-NT Software Reference Manual*, version 5.1; Bruker AXS, Inc.: Madison, WI, 1998.

(33) Piñero, D.; Raptis, R. G., unpublished results.

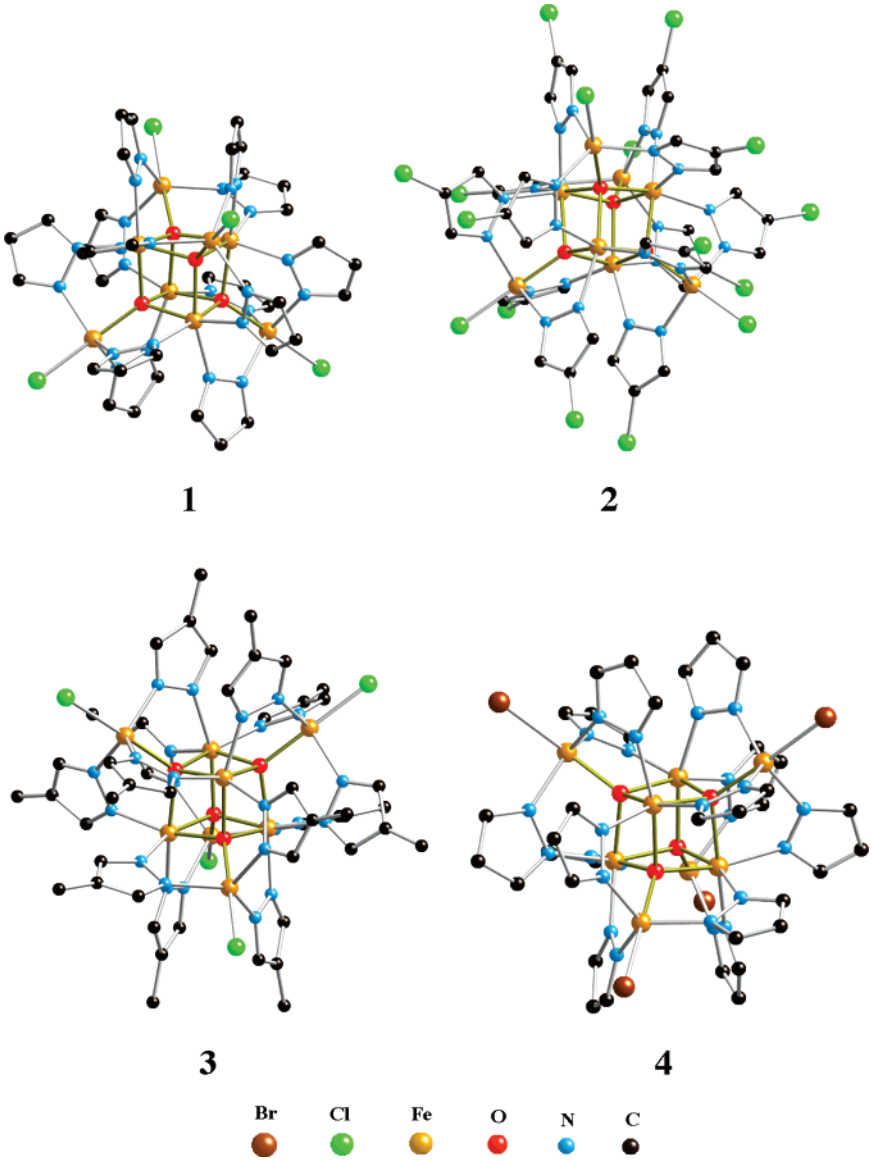

Figure 1. Ball-and-stick diagrams of **1**−**4**.

Table 2. Selected Bond Distances (Å) and Interatomic Angles (deg) for **1**−**4**

	1	**2**	**3**	**4**
Fe_c−O	2.032(6)−2.066(7)	2.047(2)	2.028(5)−2.066(5)	2.033(6)−2.060(6)
Fe_c−N	2.044(9)−2.086(8)	2.101(3)	2.044(7)−2.080(7)	2.048(9)−2.090(8)
Fe_c···Fe_c	3.067(2)−3.091(2)	3.073(2)	3.055(2)−3.112(2)	3.056(2)−3.090(2)
Fe_c−O−Fe_c	96.5(3)−98.4(3)	97.3(2)	96.6(2)−99.0(2)	96.5(2)−98.7(3)
O−Fe_c−O	81.1(3)−82.7(3)	82.2(2)	80.7(2)−82.7(2)	81.1(2)−82.9(2)
Fe_o−O	1.940(7)−1.960(6)	1.930(4)	1.950(5)−1.970(5)	1.943(6)−1.954(6)
Fe_o−X	2.271(4)−2.274(4)	2.293(2)	2.284(2)−2.291(2)	2.421(2)−2.425(2)
Fe_o−N	2.003(9)−2.038(10)	2.028(3)	2.002(7)−2.034(6)	2.008(9)−2.048(9)
O−Fe_o−X	176.9(2)−179.5(2)	180.0(1)	177.7(2)−179.4(2)	176.6(2)−178.9(2)
N−Fe_o−N	114.1(4)−124.4(4)	119.6(1)	114.5(3)−123.7(3)	113.5(3)−125.2(3)
Fe_o···Fe_o	5.841(3)−5.888(2)	5.843(2)	5.808(2)−5.954(2)	5.835(2)−5.895(2)
Fe_o···Fe_c[a]	3.425(2)−3.481(2)	3.4432(8)	3.437(2)−3.488(2)	3.426(2)−3.487(2)
Fe_o···Fe_c[a]	5.462(2)−5.483(3)	5.460(1)	5.472(2)−5.491(2)	5.457(2)−5.484(2)

[a] There are three short and one long Fe_o···Fe_c distances per Fe atom, between the vertices of co-centrical tetrahedra formed by the four Fe_c and four Fe_o atoms, respectively.

running parallel to the Cl−Fe_o−O···Fe_c axes and through the centers of opposite Fe_2O_2 faces of the cubane, respectively. Within the Fe_4O_4 cubanes, the Fe−O bonds range from 2.03 to 2.07 Å, while the Fe−O−Fe and O−Fe−O angles vary from 96.5° to 99.0° and from 80.7° to 82.9°, respectively. The Fe_2O_2 faces of the cubane cores deviate only slightly from planarity, in contrast to the Fe_2S_2-butterfly arrangement in Fe_4S_4-cubanes. Both Fe−O and Fe−N bonds

Scheme 1. $Fe_8(\mu_4\text{-}O)_4$ Motif of Complexes **1**−**4**, Ferrihydrite, Maghemite, and Ferrihydrite, Also Indicating the Cubane and Outer Fe Atoms and Numbering Scheme for the Pyrazolate Protons

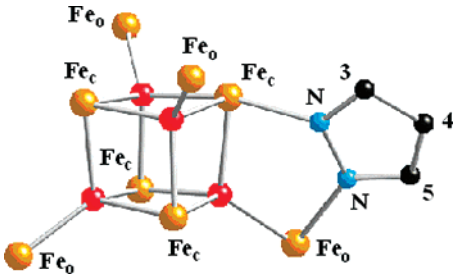

Table 3. Comparison of Structural and Mössbauer Isomer Shift Data

	1−**4**[a]	maghemite[b]	ferrihydrite[c]	magnetite[d]
Fe_c−O	2.028−2.066	2.015−2.104	1.96−2.14	2.140
$Fe_c\cdots Fe_c$	3.055−3.112	2.894−3.012	2.91−3.20	2.968
Fe_c−O−Fe_c	96.5−99.0	87.9−95.2	85.8−102.5	87.78
O−Fe_c−O	80.7−82.9	84.7−93.1	73.5−91.0	92.18
δ, mm s^{-1}	0.32(2), 293 K	0.37(5), 293 K	0.35(1), 293 K	$Fe^{2+/3+}$; 0.67, 298 K

[a] This work. [b] Reference 35. [c] Reference 34. [d] Reference 36.

are slightly shorter for the five-coordinate outer Fe-atoms (Fe_o) compared with those of six-coordinate cubane Fe atoms (Fe_c). The introduction of an electron-withdrawing (Cl, **2**) or an electron-releasing (Me, **3**) substituent at the pyrazole 4-position or the replacement of terminal chlorine by bromine ligands (**4**) have no significant effect on the structural parameters of the Fe_4O_4-cubanes, which remain practically invariant in all four structures.

The $Fe_8(\mu_4\text{-}O)_4$ motif of **1**−**4** (Scheme 1) closely resembles the $Fe_8(\mu_4\text{-}O)_4$ units present in the all-ferric minerals ferrihydrite ($Fe_5HO_8{\cdot}4H_2O$) and maghemite (γ-Fe_2O_3), and also in mixed-valent magnetite (Fe_3O_4).[34−36] The Fe_c−O bond lengths of **1**−**4** are within the range for the corresponding bonds of maghemite and ferrihydrite, but shorter than those of magnetite, consistent with the mixed-valent nature of the latter (Table 3). The $Fe_c\cdots Fe_c$ as well as the O−Fe_c−O and Fe_c−O−Fe_c angles of **1**−**4** and the three minerals are also similar. Besides ferrihydrite, maghemite, and magnetite, the $Fe_8(\mu_4\text{-}O)_4$ motif has also been found recently in the salicylaldoximate complex $Fe_8^{III}O_4(sao)_8(py)_4$ of S_4 symmetry, which contains only six-coordinate Fe atoms.[19] The irregular $Fe_4(\mu_4\text{-}O)_4$ cubane core of the latter complex has butterfly distorted Fe_2O_2 faces with Fe_c−O bond lengths in the range of 1.990−2.231 Å.

The Ga analogue of **1**, $Ga_8(\mu_4\text{-}O)_4(\mu\text{-}pz)_{12}Cl_4$, is also known.[37] As Ga^{III} and Fe^{III} have similar radii, the bond lengths and angles around the Ga centers are quite similar to those around the Fe centers of **1**.[38]

NMR Data Analysis. The solution ^{1}H NMR spectra of **1**, **3**, and **4** all show three broad, singlet, paramagnetically shifted resonances (Table 4) assigned to the pzH 3-, 4-, and

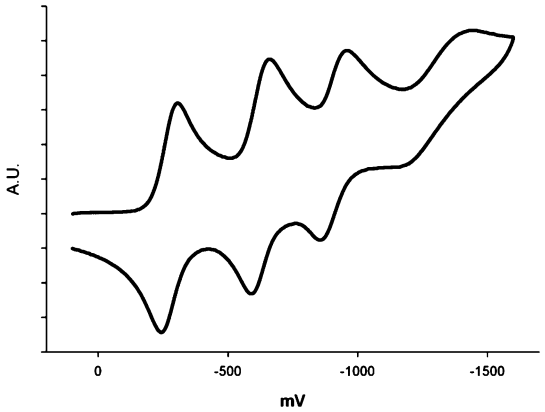

Figure 2. Cyclic voltamogram of **4** in 0.5 M Bu_4NPF_6/CH_2Cl_2, Pt-disk working electrode, vs Fc/Fc^+.

Table 4. ^{1}H NMR Data for **1**−**4**

compound	^{3}H	^{4}H	^{5}H
1	10.5	42.2	3.5
2	13.7		8.6
3	8.6	27.7 (Me^4)	3.8
4	10.7	42.9	1.0

5-positions and two resonances in the spectrum of the 4-Cl-pz complex **2** corresponding to the pzH 3- and 5-positions, consistent with their molecular formulas (Scheme 1). The magnetic equivalence of twelve pzH rings confirms the *T* molecular symmetry of all four complexes in solution. Complexes **1** and **4** differ only in their terminal halogen ligands. Their corresponding ^{1}H NMR spectra differ most significantly in their upfield resonances, 3.5 ppm for **1** and 1.0 ppm for **4**, on the basis of which we tentatively assign them to the proximal ^{5}H (position 3 is defined as the one closer to the Fe_4O_4-cubane, while position 5 is the one closer to a outer Fe centers, Scheme 1). By analogy, the upfield resonances of **2** and **3** (8.6 and 3.8 ppm) are also assigned to the ^{5}H atoms. For **3**, the peak area integration clearly identifies the methyl group downfield resonance at 27.7 ppm. Similarly, the downfield resonances of **1** and **4** (42.2 and 42.9 ppm) are also assigned to the ^{4}H atoms. This leaves the midfield resonances of all four complexes assigned to their ^{3}H atoms. The comparison of the ^{1}H NMR spectra for **1** and **2** shows the influence of the Cl atom in the 4-position of pzH; the ^{3}H and ^{5}H atoms of **2** are shifted approximately 3 and 5 ppm downfield.

Vibrational Spectroscopy. The IR spectra of **1**−**4** (Supporting Information, Section S1) consist of absorptions in the 1600−500 cm^{-1} range assigned to pzH vibrations. Additional absorptions assigned to a Fe−O stretch are observed at 475 cm^{-1} (**1**), 478 cm^{-1} (**2**), 476 cm^{-1} (**3**), and 475 cm^{-1} (**4**). In ^{18}O-labeled **2**, this band shifts to 466 cm^{-1}, confirming its assignment. An absorption assigned to a Fe−O stretch, observed in the Raman spectrum of **2** at 441 cm^{-1}, shifts to 428 cm^{-1} in the ^{18}O-labeled sample (Supporting Information, Section S2).

Electrochemistry. The electrochemical properties of complexes **2**−**4,** as determined by cyclic voltammetry, are similar to those already reported for **1**.[20] All four complexes show four reversible one-electron processes that reduce the

(34) Michel, F. M.; Ehm, L.; Antao, S. M.; Lee, P. L.; Chupas, P. J.; Liu, G.; Strongin, D. R.; Schoonen, M. A. A.; Phillips, B. L.; Parise, J. B. *Science* **2007**, *316*, 1726.
(35) (a) Greaves, C. *J. Solid State Chem.* **1983**, *49*, 325. (b) Sinha, H. P.; Sinha, A. P. B. *Z. Anorg. Allg. Chem.* **1958**, *293*, 228.
(36) Fleet, M. F. *Acta Crystallogr.* **1981**, *B37*, 917.
(37) Capparelli, M. V.; Hodge, P.; Piggott, B. *Chem. Commun.* **1997**, 937.
(38) Shannon, R. D. *Acta Crystallogr.* **1976**, *A32*, 751.

Table 5. Cyclic Voltammetric Data for Complexes **1**−**4** in Dichloromethane at 298 K

	potential, V			
	$E_{1/2}(1)$	$E_{1/2}(2)$	$E_{1/2}(3)$	$E_{1/2}(4)$
$Fe_8(\mu_4\text{-}O)_4(\mu\text{-}pz)_{12}Cl_4$ (**1**)	−0.43[a]	−0.78[a]	−1.07[a]	−1.38[a]
$Fe_8(\mu_4\text{-}O)_4(\mu\text{-}4\text{-}Cl\text{-}pz)_{12}Cl_4$ (**2**)	−0.42	−0.67	−0.96	−1.25
$Fe_8(\mu_4\text{-}O)_4(\mu\text{-}4\text{-}Me\text{-}pz)_{12}Cl_4$ (**3**)	−0.58	−0.91	−1.20	−1.55
$Fe_8(\mu_4\text{-}O)_4(\mu\text{-}pz)_{12}Br_4$ (**4**)	−0.33	−0.62	−0.89	−1.16

[a] Data from ref 20.

neutral complexes to their corresponding mono-, di-, tri-, and tetraanions (Figure 2). Inspection of the $E_{1/2}$ values of complexes **1**−**4** (Table 5) shows that substitution, both at the peripheral μ-pyrazole 4-positions as well as of the terminal halide ligands, influences the redox properties of the complex. The introduction of 12 electron-withdrawing chlorine substituents causes an anodic shift of 0.01−0.13 V in the $E_{1/2}$ values of **2** compared with those of **1**, while the introduction of 12 electron-releasing methyl group substituents causes a cathodic shift of 0.15−0.17 V in **3** compared with the values of **1**. The exchange of terminal Cl for Br ligands in **4**, on the other hand, brings about an anodic shift of 0.10−0.22 V. The fact that the two different types of substitution cause $E_{1/2}$ shifts of the same magnitude argues for the redox-active centers of the Fe_8 complexes being remote from both substitution sites, e.g., the redox activity is confined to the six-coordinate centers of the encapsulated Fe_4O_4-cubane, not the four outer five-coordinate Fe centers, which are directly connected to the terminal halide ligands. The rich redox chemistry of complexes **1**−**4** distinguishes them from other known Fe_4O_4 complexes, for which no reversible electrochemistry has been reported to date. We attribute this to the protection afforded by the outer, inert shell, consisting of four Fe(μ-pz)$_3$ units to the redox-active Fe_4O_4 core of **1**−**4**.

The separation measured here between the first and fourth redox process of each Fe_8 complex, $\Delta E_{1-4} = 0.95$ V (**1**), 0.83 V (**2** and **4**), and 0.97 V (**3**), is much larger than the theoretical $\Delta E_{1-4} = 0.0712$ V separation in a system of four noninteracting redox centers.[39] While the degree of electronic communication among Fe centers cannot be determined from the separation of $E_{1/2}$ values (solvation and ion-pairing effects can significantly influence $E_{1/2}$ values), the $\Delta E_{n-(n+1)}$ values of **1**−**4** indicate some degree of valence delocalization. A qualitative comparison between isovalent $\Delta E_{n-(n+1)}$ values of Fe_4O_4 and Fe_4S_4 cubanes shows a larger separation between consecutive redox processes in the latter, evidence of a higher degree of charge delocalization in the iron−sulfur clusters. The narrow ΔE_{1-4} separation of 0.83−0.97 V found here for Fe_4O_4 cubanes means that they can shuttle four electrons across a narrower redox potential window than the corresponding Fe_4S_4 cubanes; Fe_4O_4 cubanes are more efficient electron-transfer agents. As electron acceptors, the Fe_8 complexes **1**−**4** are more efficient than C_{60}, for which the first four redox processes are separated by 0.43−0.53 V, giving a ΔE_{1-4} value of 1.41 V.[40]

(39) Flanagan, J. B.; Margel, S.; Bard, A. J.; Anson, F. C., *J. Am. Chem. Soc.* **1978**, *100*, 4248.

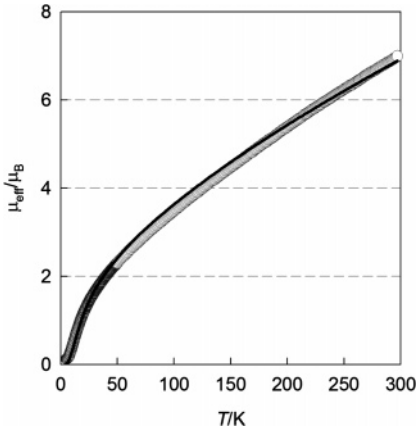

Figure 3. Temperature dependence of the effective magnetic moment for **1**. Open circles, experimental data; full points, calculated.

Analysis of Magnetic Data of 1. The effective magnetic moment, μ_{eff}, at $T = 300$ K is 7.0 μ_B, and on cooling this gradually descends to 0.12 μ_B at $T = 2.0$ K (Figure 3). The value at room temperature is much smaller than that expected for eight uncoupled Fe^{III} centers with $g = 2.0$ ($\mu_{eff} = 16.7$ μ_B), and the decrease of the magnetic susceptibility upon cooling confirms the presence of strong antiferromagnetic exchange interaction in **1**. The inverse susceptibility is nonlinear, as a result of these exchange interactions which result in an unequal population of energy levels.

In order to interpret the magnetic properties, the following spin Hamiltonian was postulated:

$$\hat{H} = -J_1\sum_{i=1}^{4}\sum_{j>i}^{4}\mathbf{S}_i\cdot\mathbf{S}_j - J_2\sum_{k=1,2,3}\mathbf{S}_5\cdot\mathbf{S}_k - J_2\sum_{k=1,2,4}\mathbf{S}_6\cdot\mathbf{S}_k - J_2\sum_{k=2,3,4}\mathbf{S}_7\cdot\mathbf{S}_k - J_2\sum_{k=1,3,4}\mathbf{S}_8\cdot\mathbf{S}_k + \mu_B\sum_{i=1}^{8}\mathbf{S}_i\cdot\mathbf{g}_i\cdot\mathbf{B} \quad (1)$$

where J_1 represents the isotropic exchange interactions in the $Fe^{III}{}_4O_4$-cubane core mediated only through μ_4-O bridges, J_2 represents the isotropic exchange interactions between each apical Fe^{III} center and the triangular base of the inner tetrahedron to which it lies closest, mediated through μ_4-O and μ-pz bridges (Scheme 2), and the last term is the Zeeman term. We have ignored the coupling between the outer Fe centers, which is expected to be small due to the large internuclear separation.

The exchange coupling of eight Fe^{III} centers, each with the local spin $S_i = {}^5/_2$, leads to $(2S_i + 1)^8 = 6^8 = 1\,679\,616$ magnetic states with total spin ranging from $S = 0$ to $S = 20$. Unfortunately, the postulated spin Hamiltonian is not symmetric, and it is not possible to obtain an analytical formula for energy levels. Moreover, it is not feasible to efficiently diagonalize such large interaction matrices. To reduce the dimensions of the matrices, we have focused on the total spin symmetry principle (TSSP) for which the conditions (g factors equal for all magnetic centers and no nonisotropic terms present) are fulfilled.[41] In order to take advantage of the TSSP approach, it is necessary to calculate

(40) (a) Xie, Q.; Pérez-Cordero, E.; Echegoyen, L. *J. Am. Chem. Soc.* **1992**, *114*, 3978. (b) Ohsawa, Y.; Saji, T. *J. Chem. Soc., Chem. Commun.* **1992**, 781.

Scheme 2. Alignment of the Spin Vectors in HS, BS1, and BS2 Configurations

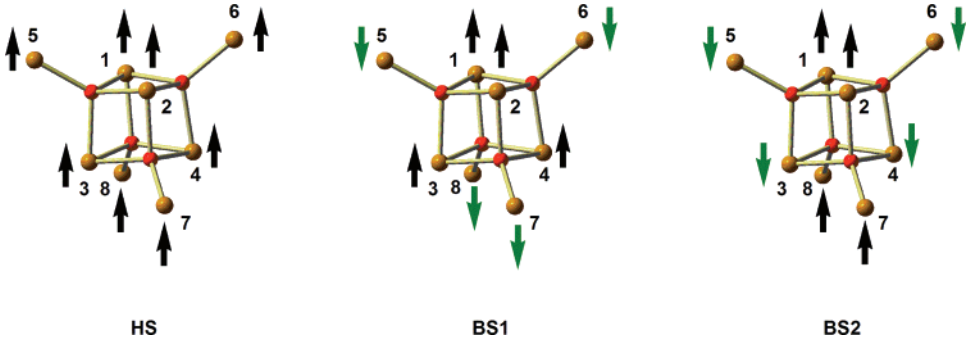

energy values in the coupled basis set labeled as $|\alpha SM\rangle$ using irreducible tensor operators,[42] where α stands for the intermediate quantum numbers denoting the coupling path. First, only the isotropic exchange terms are involved, and the whole matrix is factorized into the blocks according to the final spin quantum number S. As a result, the energies in zero magnetic field are obtained. The largest dimension of the submatrix is 16 576 for $S = 5$ (Supporting Information, Section S3). Consequently, the energy levels in nonzero magnetic field are calculated as $E_i(\alpha SM) = E_{0,i}(\alpha S) + \mu_B gBM$. Nowadays, this approach is feasible on modern computers, but it takes a few days to calculate the whole energy spectrum. Obviously, this procedure is not suitable for fitting of the magnetic data, and further reduction of the dimensions of the matrices is needed.

To solve this problem, the spin permutational symmetry (SPS) of the spin Hamiltonian was applied[41] and the energy levels were classified (Supporting Information, Section S3) according to the irreducible representation of the D_2 point group (D_2 is a subgroup of the local T_d symmetric Fe_8O_4 core). Numerically efficient use of the SPS approach demands a coupling scheme, which is left invariant under the symmetry operations of the point group. This condition is fulfilled for $\mathbf{S}_{12} = \mathbf{S}_1 + \mathbf{S}_2$, $\mathbf{S}_{34} = \mathbf{S}_3 + \mathbf{S}_4$, $\mathbf{S}_{56} = \mathbf{S}_5 + \mathbf{S}_6$, $\mathbf{S}_{78} = \mathbf{S}_7 + \mathbf{S}_8$, $\mathbf{S}_{1234} = \mathbf{S}_{12} + \mathbf{S}_{34}$, $\mathbf{S}_{5678} = \mathbf{S}_{56} + \mathbf{S}_{78}$, and $\mathbf{S} = \mathbf{S}_{1234} + \mathbf{S}_{5678}$. As a result, each exchange matrix for final spin S is further factorized in relation to the irreducible representation of the D_2 point group. Now, the largest matrix has the dimension of 4201 for $S = 4$ and $\Gamma = A_1$ and calculation of the whole energy spectrum is much faster (Supporting Information, Section S3).

With the energy levels labeled as $E_i(\alpha SM,\Gamma_j) = E_{0,i}(\alpha S,\Gamma_j) + \mu_B gBM$, the molar magnetization can be easily calculated as

$$M_{\mathrm{mol}} = N_A \mu_B gB \frac{\sum_i M \exp[-E_i(\alpha SM,\Gamma_j)/kT]}{\sum_i \exp[-E_i(\alpha SM,\Gamma_j)/kT]} \qquad (2)$$

Fitting the experimental magnetization to this expression resulted in the following set of parameters: $J_1/\mathrm{hc} = -2.1$ cm^{-1} and $J_2/\mathrm{hc} = -50.6$ cm^{-1} with fixed $g = 2.0$. The fitting procedure was rather insensitive to the (small) value and sign of the coupling constant J_1. The grid of error functional R,[43] for varying J_1 and J_2 parameters, was calculated to confirm that the solution is the global minima (Supporting Information, Section S3). Also, the standard deviations were calculated for fitted parameters with 95% probability and resulted in $J_1/\mathrm{hc} = -2.1 \pm 2.6$ cm^{-1} and $J_2/\mathrm{hc} = -50.55 \pm 0.24$ cm^{-1}.

The large negative value of J_2 indicates significant antiferromagnetic coupling between the inner and outer magnetic centers and is consistent with the magnetic measurements. The magnetic interaction in the Fe_4O_4 cubane core is weak and most probably antiferromagnetic in nature, although the possibility of a very small ferromagnetic interaction cannot be excluded on the basis of the magnetic properties.

The reconstructed energy levels in zero magnetic field as a function of final spin S are shown in Figure 4. The ground state is $S = 0$, and it is evident that the rotational band is retained for the bottom level of each spin, which is expected for antiferromagnetic coupled clusters.[44] Obviously, only a very limited part of the energy spectrum is thermally populated, explaining the deviation of magnetic susceptibility from the Curie−Weiss law.

Electronic Structure of 1. To shed further light on the magnetic interactions in the parent cluster $Fe_8(\mu_4\text{-}O)_4(\mu\text{-}pz)_{12}Cl_4$, we have explored its electronic structure using spin-unrestricted DFT (B3LYP functional). Using the crystallographically determined geometry, we have computed the energies of three distinct electronic configurations (Scheme

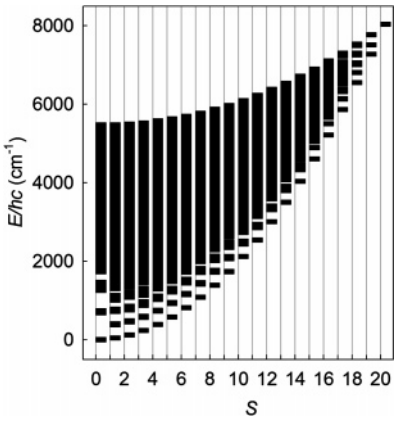

Figure 4. Energy levels versus spin for **1** at $B = 0$.

(41) Waldmann, O. *Phys. Rev. B: Condens. Matter Mater. Phys.* **2000**, *61*, 6138.
(42) Boča, R. *Theoretical Foundations of Molecular Magnetism*; Elsevier: Amsterdam, 1999.

Table 6. Computed Net Spin Densities and Total Energies of Fe_c and Fe_o Centers

	$\rho(Fe_c)$	$\rho(Fe_o)$	$\langle S^2\rangle$	E/au
BS1 ($M_S = 0$)	4.18	−4.03	19.47	−4055.4684
BS2 ($M_S = 0$)	±4.20	±4.03	19.54	−4055.4578
HS ($M_S = 20$)	4.18	4.03	420.07	−4055.4323

2), differing in the relative orientations of the spin vectors. The first of these, the high-spin state (HS), has $M_S = 20$, while the two broken-symmetry states, BS1 and BS2, have $M_S = 0$.

$$\text{HS,}\quad |^5/_2\rangle|^5/_2\rangle|^5/_2\rangle|^5/_2\rangle|^5/_2\rangle|^5/_2\rangle|^5/_2\rangle|^5/_2\rangle$$

$$\text{BS1,}\quad |^5/_2\rangle|^5/_2\rangle|^5/_2\rangle|^5/_2\rangle|-^5/_2\rangle|-^5/_2\rangle|-^5/_2\rangle|-^5/_2\rangle$$

$$\text{BS2,}\quad |^5/_2\rangle|^5/_2\rangle|-^5/_2\rangle|-^5/_2\rangle|-^5/_2\rangle|-^5/_2\rangle|^5/_2\rangle|^5/_2\rangle$$

In BS1, the spin vectors on the inner core are aligned parallel to each other (ferromagnetic), but antiparallel to those on the outer iron centers. In contrast, in BS2 the Fe_4O_4 core is subdivided into a "dimer-of-dimers" structure, with the spins on the upper half aligned antiparallel to those on the lower half (similar models of electronic structure have been used to describe the antiferromagnetic coupling in Fe_4S_4 cubanes).[45] The outer tetrahedron is similarly divided into upper and lower halves, with the spin vectors aligned antiparallel to those in the Fe_4O_4 core.

Applying the Heisenberg spin Hamiltonian

$$\hat{H} = -J_1\sum_{i=1}^{4}\sum_{j>i}^{4} S_i\cdot S_j - J_2\sum_{k=1,2,3} S_5\cdot S_k - J_2\sum_{k=1,2,4} S_6\cdot S_k - J_2\sum_{k=2,3,4} S_7\cdot S_k - J_2\sum_{k=1,3,4} S_8\cdot S_k \quad (3)$$

to each of these three single determinant wavefunctions gives the following expressions for energies:

$$E(\text{HS}) = -\frac{150}{4}J_1 - \frac{300}{4}J_2,\quad E(\text{BS1}) = -\frac{150}{4}J_1 + \frac{300}{4}J_2,\quad E(\text{BS2}) = +\frac{50}{4}J_1 + \frac{100}{4}J_2$$

from which the expressions for J_1 and J_2 can be derived:

$$J_2 = \frac{E(\text{BS1}) - E(\text{HS})}{150}\ \text{and}\quad J_1 = \frac{3E(\text{BS2}) - 2E(\text{BS1}) - E(\text{HS})}{150}$$

The computed total energies and net spin densities at each iron center are summarized in Table 6, along with expectation values of the square of the total spin operator, $\langle S^2\rangle$. Spin densities of 4.0−4.2 are typical of high-spin Fe^{III} centers, while the values of $\langle S^2\rangle$ are close to the ideal values for ferromagnetic ($\langle S^2\rangle = 420$) and broken-symmetry ($\langle S^2\rangle = 20$) states arising from the coupling between eight $S = {}^5/_2$ single ions.

The resulting calculated values of $J_1/hc = -6.3\ cm^{-1}$ and $J_2/hc = -52.8\ cm^{-1}$ are in excellent agreement with the experimental values of -2.1 and $-50.6\ cm^{-1}$, respectively, and confirm the dominance of antiferromagnetic coupling between the inner and outer Fe centers, mediated by the μ_4-O bridges. The much stronger antiferromagnetic coupling between the inner and outer iron centers is related to the larger angles subtended at the bridging oxide ligands (119°), a result of which the Fe_c-O-Fe_o superexchange pathway is more efficient than Fe_c-O-Fe_c, where the angles are closer to 90° (98°). The partial delocalization of the Fe_o d_{z^2} electron onto the Fe_c center is apparent in the contour plot of the highest occupied molecular orbital (HOMO) of BS2 (shown in Figure 5). We note that Murrie and co-workers have reported similar antiferromagnetism in their $[Fe_8^{III}O_4(sao)_8(py)_4]\cdot 4py$ system and proposed that the dominant exchange pathway is also mediated by the μ_4-O ligands.[19]

The localization of the molecular orbitals around the frontier region also sheds some light on the observed electrochemical properties. In each case (HS, BS1, and BS2), the lowest vacant orbitals are largely localized on the inner Fe_4O_4 core (HOMO and LUMO are shown for the BS2 state in Figure 5), consistent with our proposal that this is the site of the four reduction processes. There is, however, some significant delocalization onto the outer Fe centers, Fe_o, which would lead to a buffering of the electronic effects of successive reductions, as proposed by Lippard et al.[15]

Mössbauer Spectroscopy. At zero magnetic field, the Mössbauer spectra of **1** consist of two quadrupole doublets in the 4.2−300 K temperature range. The zero field spectrum recorded at 4.2 K is shown in Figure 6. The deconvolution of the zero field spectra may be carried out assuming two different models with either two "nested" (Figure 6) or two "crossed" doublets (Supporting Information, Section S4). The parameters obtained by the two methods are listed in Table 7. For either model, it is ascertained that the isomer shift values in the whole temperature range fall in the range of high-spin ferric ions in an octahedral environment with N/O donors (the decrease in the values of isomer shifts from 4.2 to 293 K is attributed to a second-order Doppler effect[46]). Moreover, for both models, the site with the lower isomer shift value (A, $\delta = 0.37$ and 0.32 mm s^{-1} at 4.2 K) is characterized by the largest quadrupole splitting (B, $|\Delta E_Q| = 0.68$ and 0.57 mm s^{-1}).

The Mössbauer parameter values strongly indicate that site A corresponds to the five-coordinate peripheral ions, Fe_o, whereas site B corresponds to the six-coordinate cubane ferric ions, Fe_c.[46] The decrease of the isomer shift upon decrease of coordination number is associated with a decrease of the

(43) The error functional is defined as $R = 100/N \times \sum_{i}^{N}(1 - \mu^c_{\text{eff},i}/\mu^o_{\text{eff},i})$, where $\mu^c_{\text{eff},i}$ is calculated effective moment, $\mu^o_{\text{eff},i}$ is observed effective moment, and N is number of experimental points.

(44) Schnack, J.; Luban, M. *Phys. Rev. B*: *Condens. Matter Mater. Phys.* **2001**, *B63*, 014418.

(45) (a) Noodleman, L.; Case, D. A. *Adv. Inorg. Chem.* **1992**, *38*, 423. (b) Aizman A.; Case D. A. *J. Am. Chem. Soc.* **1982**, *104*, 3269. (c) Noodleman, L.; Peng, C. Y.; Case D. A.; Mouesca J.-M. *Coord. Chem. Rev.* **1995**, *144*, 199.

(46) Greenwood, N. N.; Gibb, T. C. *Mössbauer Spectroscopy*; Chapman and Hall, Ltd.: London, 1971.

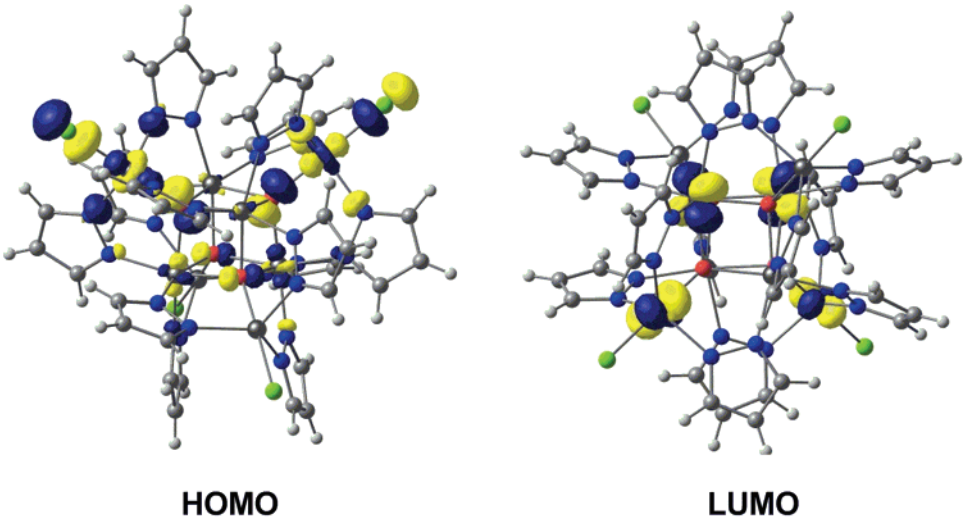

Figure 5. Contour plot of the spin-α HOMO and LUMO for the BS2 state of **1**.

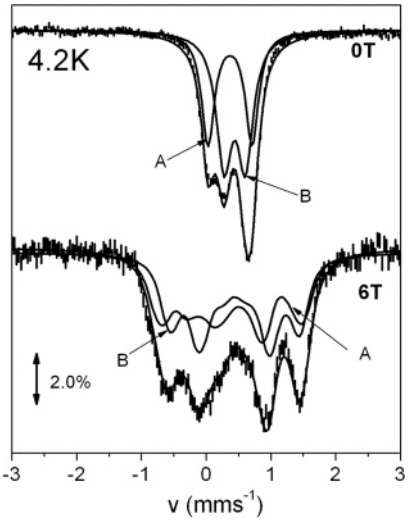

Figure 6. Mössbauer spectra from powdered samples of **1** in the absence or presence of an external magnetic field of 6 T applied perpendicular to the γ-rays. Solid lines are theoretical simulations assuming two species A and B with the parameters quoted in Table 7 (nested model).

Table 7. Mössbauer Hyperfine Parameters of **1** at 4.2 K (293 K) for the Two Different Deconvolution Models

model	site	δ (mm s^{-1})[a]	$\lvert\Delta E_Q\rvert$ (mm s^{-1})[b]	η	assignment
nested	A	0.37 (0.25)	0.68 (0.65)	<0.6	Fe_o
	B	0.44 (0.32)	0.33 (0.30)	<0.7	Fe_c
crossed	A	0.32 (0.19)	0.57 (0.52)	<0.6	Fe_o
	B	0.50 (0.36)	0.43 (0.38)	<0.3	Fe_c

[a] (±0.01 mm s^{-1}). [b] (±0.02 mm s^{-1}).

bond length, as it appears for the peripheral ferric ions with bond lengths slightly shorter than those of the cubane. The symmetry of the peripheral Fe_o centers is lower than that of the cubane ones, Fe_c, and this is reflected in the larger ΔE_Q value of site A in both models.[47] Values of δ similar to those of Fe_c of **1** with *fac*-O_3N_3 coordination have been observed in the low-temperature spectra of a mononuclear complex with *cis*-O_2N_4 coordination (δ = 0.44 mm s^{-1} at 80 K), a dinuclear complex containing a Fe_2O_2 core with O_6 and O_5N coordination (δ = 0.45 mm s^{-1} at 4.2 K), and horse spleen ferritin (δ = 0.45 mm s^{-1} at 100 K).[48−50] Furthermore, compared to the minerals ferrihydrite and maghemite, **1** exhibits similarity in both structure and Mössbauer isomer shifts (Table 3) .[51,52]

From the analysis of the magnetic susceptibility measurements for **1**, a diamagnetic (S = 0) ground state is inferred with a S = 1 excited state ~39 cm^{-1} higher in energy. An isolated ground state with S = 0 is further supported by the Mössbauer spectra. In Figure 6 we show a spectrum recorded at 4.2 K in the presence of an external magnetic field of 6 T applied perpendicular to the γ-rays.

In an exchange coupled system, the local magnetic field induced on each ferric site of the cluster is given by

$$\mathbf{B}_{tot} = \mathbf{B}_{ext} + \mathbf{B}_{int} \quad (4)$$

where $\mathbf{B}_{ext}$ is the applied magnetic field and $\mathbf{B}_{int} = -a_i\langle \mathbf{S}_i\rangle / g_n\beta_n$; a_i is the intrinsic hyperfine tensor for a ferric ion and $\langle \mathbf{S}_i\rangle$ is the spin expectation value for each ferric ion and critically depends on the total spin S of each multiplet of the exchange coupled system and the exchange coupling scheme. For states with total spin S = 0, $\langle \mathbf{S}_i\rangle$ = 0. In such cases, each ferric ion nucleus will experience only the external field $\mathbf{B}_{ext}$. The magnetically perturbed spectrum of Figure 6 can be readily simulated assuming two sites with $\mathbf{B}_{int}$ = 0 (within experimental error) indicating that the ground state of the cluster is diamagnetic, well isolated from states with nonzero total spin. We have fitted the magnetically perturbed spectrum assuming both models (nested or crossed), and better results were obtained assuming the nested one (shown in Figure 6). Finally, the analysis of the magnetically perturbed spectra allowed for the estimation

(47) Bill, E.; Krebs, C.; Winter, M.; Gerdan, M.; Trautwein, A. X.; Flörke, U.; Haupt, H.-J.; Chaudhuri, P. *Chem.—Eur. J.* **1997**, *3*, 193.

(48) Benisvy, L.; Halut, S.; Donnadieu, B.; Tuchagues, J.-P.; Chottard, J.-C.; Li, Y. *Inorg. Chem.* **2006**, *45*, 2403.
(49) Yoon, S.; Lippard, S. J. *J. Am. Chem. Soc.* **2004**, *126*, 2666.
(50) Watt, G. D.; Frankel, R. B.; Papaefthymiou, G. C. *Proc. Natl. Acad. Sci. U.S.A.* **1985**, *82*, 3640.
(51) Murad, E.; Bowen, L. H.; Long, G. L.; Quin, T. G. *Clay Miner.* **1988**, *23*, 161.
(52) Annersten, H.; Hafner, S. S. *Z. Kristallogr.* **1973**, *137*, 321.

of the asymmetry parameter η of the electric field gradient tensor along with the determination of the sign of the quadrupole splitting. For both deconvolution models, the quadrupole splitting is found to be negative.

Conclusions

The crystal structures of the octanuclear complexes **1**−**4** show that the 3- and 5-positions of pzH ligands are sterically hindered in these materials, while the 4-position radiates unhindered from the approximately spherical structure. Further property tuning in the family of $Fe_8(\mu_4\text{-}O)_4$-containing compounds can be achieved by the introduction of appropriate substituents at the pzH 4-position, as has been shown here for the redox properties of **1**−**3**.

There have been only a few examples of polynuclear Fe^{III} clusters of which the magnetic properties have been thoroughly analyzed to date.[53] The main theoretical complication lies in the very high number of spin states; this problem can be solved gracefully by using the symmetry of the spin Hamiltonian, which was successfully presented in the Article. Analysis of the temperature dependence of the magnetic susceptibility indicates the presence of strong antiferromagnetic coupling between the inner and outer Fe centers, with rather weaker coupling within the Fe_4O_4 core. The computed electronic structure of the cluster confirms the presence of highly localized high-spin Fe^{III} centers and also the dominance of the superexchange pathway between core and outer iron centers, mediated by the μ_4-O bridge. Furthermore, although the lowest-lying vacant orbitals are found to be largely localized on the core irons, significant delocalization onto the outer metal centers will buffer the redox events to some extent, possibly accounting for the very narrow window over which the four one-electron reduction steps occur.

The $M_8(\mu_4\text{-}O)_4$ motif is common in metal complexes, as well as in minerals. Complexes in which the $M_8(\mu_4\text{-}O)_4$ core is supported by 12 bridging ligands are known in both carboxylate (M = Cr,[54] Co,[55] V/Zn,[56] Fe[19]) and pyrazolate systems (M = Ga,[30] Fe; Scheme 1). The Fe^{III} minerals maghemite and ferrihydrite and the $Fe^{III/II}$ magnetite contain $Fe_8(\mu_4\text{-}O)_4$ units. In the extended structures of all three of those minerals, the six-coordinate Fe_c vertices are shared between two consecutive cubanes, while the Fe_o vertices are *tetrahedrally* coordinated by four μ_4-O atoms of four cubane units (while the Fe_o centers of **1**−**4** are *trigonal bipyramidal*). In contrast, in the structures of **1**−**4** the 12 pz bridges and the 4 terminal halogen atoms block all the remaining coordination sites of the $Fe_8(\mu_4\text{-}O)_4$ core, arresting its polymeric growth. The structural similarity between the iron-oxide cores of ferritin and ferrihydrite has been known for quite some time.[57] The further similarity between ferrihydrite and the core of complexes **1**−**4** described here implies that the latter are models of the building units of ferritin.

The present study has established the structural, spectroscopic, electrochemical, and magnetic properties and electronic structure of the all-ferric Fe_4O_4-cubane core, providing the respective "fingeprints", which may allow the recognition of this species in Nature, if indeed it exists. Ferrihydrite, maghemite, and magnetite are possible sources from which intact $Fe_8(\mu_4\text{-}O)_4$ units might be extruded by proteins. An electron-transfer protein based on a redox-active Fe_4O_4-cubane core may of course exist in an all-ferric state or any of the four reduced mixed-valent or all-ferrous states. The full characterization of pyrazolate complexes containing redox-modified Fe_4O_4-cubanes as well as a detailed investigation of the evolution of the electronic structure on reduction is currently underway in our laboratories.

Acknowledgment. Financial support from the following agencies is gratefully acknowledged: Puerto Rico, NIH-SCoRE S06GM008102; Slovakia, VEGA 1/2453/05, APVT 20-005204, and VEGA 1/3584/06; Czech Republic, the Czech Ministry of Education, Youth and Sports Grant No. MSM6198959218.

Supporting Information Available: Representative infrared and Raman spectra, detailed description of magnetic susceptibility fitting, representative Mössbauer spectrum (crossed model) (Sections S1−S5, in PDF format); and crystallographic information files for complexes **1**−**4**. This material is available free of charge via the Internet at http://pubs.acs.org.

IC7020337

(53) (a) Waldmann, O.; Koch, R.; Schromm, S.; Schülein, J.; Müller, P.; Bernt, I.; Saalfrank, R. W.; Hampel, F.; Balthes, E. *Inorg. Chem.* **2001**, *40*, 2986. (b) Mukhin, A.; Gorshunov, B.; Dressel, M.; Sangregorio, C.; Gatteschi, D. *Phys. Rev. B: Condens. Matter Mater. Phys.* **2001**, *63*. (c) Barra, L.; Caneschi, A.; Cornia, A.; de Biani, F.; Gatteschi, D.; Sangregorio, C.; Sessoli, R.; Sorace, L. *J. Am. Chem. Soc.* **1999**, *121*, 5302. (d) Barra, A.-L.; Bencini, F.; Caneschi, A.; Gatteschi, D.; Paulsen, C.; Sangregorio, C.; Sessoli, R.; Sorace, L. *Chem. Phys. Chem.* **2001**, *2*, 523. (e) Benelli, C.; Cano, J.; Journaux, Y.; Sessoli, R.; Solan, G. A.; Winpenny, R. E. P. *Inorg. Chem.* **2001**, *40*, 188. (f) Gatteschi, D.; Caneschi, A.; Sessoli, R.; Cornia, A. *Chem. Soc. Rev.* **1996**, *25*, 101. (g) Delfs, C.; Gatteschi, D.; Pardi, L.; Sessoli, R.; Wieghardt, K.; Hanke, D. *Inorg. Chem.* **1993**, *32*, 3099.

(54) Atkinson, I. M.; Benelli, C.; Murrie, M.; Parsons, S.; Winpenny, R. E. P. *Chem. Commun.* **1999**, 285.

(55) Dimitrou, K.; Sun, J.-S.; Folting, K.; Christou, G. *Inorg. Chem.* **1995**, *34*, 4160.

(56) Cotton, F. A.; Duraj, S. A.; Roth, W. J. *Inorg. Chem.* **1984**, *23*, 4042.

(57) Ford, G. C.; Harrison, P. M.; Rice, D. W.; Smith, J. M. A.; Treffry, A.; White, J. L.; Yariv, J. *Philos. Trans. R. Soc. London* **1984**, *B304*, 551.